Eden, D J, Liu, Tie, Kim, Kee-Tae, Juvela, M, Liu, S -Y, Tatematsu, K, Di Francesco, J, Wang, K, Wu, Y, Thompson, M A, Fuller, G A, Li, Di, Ristorcelli, I, Kang, Sung-ju, Hirano, N, Johnstone, D, Lin, Y, He, J H, Koch, P M, Sanhueza, Patricio, Qin, S -L, Zhang, Q, Goldsmith, P F, Evans, N J, Yuan, J, Zhang, C -P, White, G J, Choi, Minho, Won Lee, Chang, Toth, L V, Mairs, S, Yi, H -W, Tang, M, Soam, A, Peretto, N , Samal, M R, Fich, M, Parsons, H, Malinen, J, Bendo, G J, Rivera-Ingraham, A, Liu, H -L, Wouterloot, J, Li, P S, Qian, L, Rawlings, J, Rawlings, M G, Feng, S, Wang, B, Li, Dalei, Liu, M, Luo, G, Marston, A P, Pattle, K M, Pelkonen, V -M, Rigby, A J, Zahorecz, S, Zhang, G, Bgner, R, Aikawa, Y, Akhter, S, Alina, D, Bell, G, Bernard, J -P, Blain, A, Bronfman, L, Byun, D -Y, Chapman, S, Chen, H -R, Chen, M, Chen, W -P, Chen, X, Chen, Xuepeng, Chrysostomou, A, Chu, Y -H, Chung, E J, Cornu, D, Cosentino, G, Cunningham, M R, Demyk, K, Drabek-Maunder, E , Doi, Y, Eswaraiah, C, Falgarone, E, Fehér, O, Fraser, H, Friberg, P, Garay, G, Ge, J X, Gear, W K , Greaves, J , Guan, X, Harvey-Smith, L, Hasegawa, T, He, Y, Henkel, C, Hirota, T, Holland, W, Hughes, A, Jarken, E, Ji, T -G, Jimenez-Serra, I, Kang, Miju, Kawabata, K S, Kim, Gwanjeong, Kim, Jungha, Kim, Jongsoo, Kim, S, Koo, B -C, Kwon, Woojin, Kuan, Y -J, Lacaille, K M, Lai, S -P, Lee, C F, Lee, J -E, Lee, Y -U, Li, H, Lo, N, Lopez, J A P, Lu, X, Lyo, A -R, Mardones, D, McGehee, P, Meng, F, Montier, L, Montillaud, J, Moore, T J T, Morata, O, Moriarty-Schieven, G H, Ohashi, S, Pak, S, Park, Geumsook, Paladini, R, Pech, G, Qiu, K, Ren, Z -Y, Richer, J, Sakai, T, Shang, H, Shinnaga, H, Stamatellos, D, Tang, Y -W, Traficante, A, Vastel, C, Viti, S, Walsh, A, Wang, H, Wang, J, Ward-Thompson, D, Whitworth, A , Wilson, C D, Xu, Y, Yang, J, Yuan, Y -L, Yuan, L, Zavagno, A, Zhang, C, Zhang, G, Zhang, H -W, Zhou, C, Zhou, J, Zhu, L and Zuo, P 2019. SCOPE: SCUBA-2 Continuum observations of pre-protostellar evolution - Survey description and compact source catalogue. Monthly Notices of the Royal Astronomical Society 485 (2) , pp. 2895-2908. 10.1093/mnras/stz574

SCOPE: SCUBA-2 Continuum Observations of Pre-protostellar Evolution – Survey Description and Compact Source Catalogue

D. J. Eden,[1,2⋆] Tie Liu,[3,4] Kee-Tae Kim,[3] M. Juvela,[5] S.-Y. Liu,[6] K. Tatematsu,[7] J. Di Francesco,[8,9] K. Wang,[10] Y. Wu,[11] M.A. Thompson,[2] G.A. Fuller,[12] Di Li,[13,14] I. Ristorcelli,[15] Sung-ju Kang,[3] N. Hirano,[6] D. Johnstone,[8,9] Y. Lin,[16] J.H. He,[17,18,19] P.M. Koch,[6] Patricio Sanhueza,[7] S.-L. Qin,[20] Q. Zhang,[21] P.F. Goldsmith,[22] N.J. Evans II,[3,23] J. Yuan,[13] C.-P. Zhang,[13], G.J. White,[24,25] Minho Choi,[3] Chang Won Lee,[3,26] L.V. Toth,[27,28] S. Mairs,[4] H.-W. Yi,[29] M. Tang,[20] A. Soam,[3,30] N. Peretto,[31] M.R. Samal,[32,33] M. Fich,[34] H. Parsons,[4] J. Malinen,[35] G.J. Bendo,[12] A. Rivera-Ingraham,[36] H.-L. Liu,[37,38,39] J. Wouterloot,[4] P.S. Li,[40] L. Qian,[13] J. Rawlings,[41] M.G. Rawlings,[4] S. Feng,[42] B. Wang,[13] Dalei Li,[43] M. Liu,[13] G. Luo,[13] A.P. Marston,[44] K.M. Pattle,[45] V.-M. Pelkonen,[5,46] A.J. Rigby,[31] S. Zahorecz,[47,48] G. Zhang,[13] R. Bőgner,[27] Y. Aikawa,[49] S. Akhter,[50] D. Alina,[51] G. Bell,[4] J.-P. Bernard,[15] A. Blain,[52] L. Bronfman,[19] D.-Y. Byun,[3] S. Chapman,[53] H.-R. Chen,[54] M. Chen,[8] W.-P. Chen,[32] X. Chen,[55] Xuepeng Chen,[56] A. Chrysostomou,[57] Y.-H. Chu,[6] E.J. Chung,[3] D. Cornu,[46] G. Cosentino,[41] M.R. Cunningham,[50] K. Demyk,[15] E. Drabek-Maunder,[31] Y. Doi,[58] C. Eswaraiah,[54] E. Falgarone,[59] O. Fehér,[27,60] H. Fraser,[24] P. Friberg,[4], G. Garay,[19], J.X. Ge,[19] W.K. Gear,[31] J. Greaves,[31] X. Guan,[61] L. Harvey-Smith,[50,62] T. Hasegawa,[7] Y. He,[63] C. Henkel,[16,64] T. Hirota,[7] W. Holland,[65] A. Hughes,[15] E. Jarken,[63], T.-G. Ji,[29] I. Jimenez-Serra,[66] Miju Kang,[3] K.S. Kawabata,[67,68], Gwanjeong Kim,[7], Jungha Kim,[29] Jongsoo Kim,[3] S. Kim,[3] B.-C. Koo,[69], Woojin Kwon,[3,70] Y.-J. Kuan,[71] K.M. Lacaille,[53,72] S.-P. Lai,[6,54] C.F. Lee,[6], J.-E. Lee,[29], Y.-U. Lee,[3] H. Li,[73] N. Lo,[19] J.A.P. Lopez,[50] X. Lu,[7] A.-R. Lyo,[3] D. Mardones,[19] P. McGehee,[74] F. Meng,[61] L. Montier,[15] J. Montillaud,[46] T.J.T. Moore,[1] O. Morata,[6] G.H. Moriarty-Schieven,[8] S. Ohashi,[7] S. Pak,[29] Geumsook Park,[3] R. Paladini,[74] G. Pech,[6] K. Qiu,[75] Z.-Y. Ren,[13] J. Richer,[76] T. Sakai,[77] H. Shang,[6] H. Shinnaga,[78] D. Stamatellos,[79] Y.-W. Tang,[6] A. Traficante,[80] C. Vastel,[15] S. Viti,[41] A. Walsh,[81] H. Wang,[56] J. Wang,[55] D. Ward-Thompson,[79] A. Whitworth,[31] C.D. Wilson,[72] Y. Xu,[56] J. Yang,[56] Y.-L. Yuan,[23] L. Yuan,[13] A. Zavagno,[82] C. Zhang,[20] G. Zhang,[13] H.-W. Zhang,[11] C. Zhou,[56] J. Zhou,[63] L. Zhu,[13] and P. Zuo,[13]

Affiliations are listed at the end of the paper

Accepted XXX. Received YYY; in original form ZZZ

ABSTRACT

We present the first release of the data and compact-source catalogue for the JCMT Large Program SCUBA-2 Continuum Observations of Pre-protostellar Evolution (SCOPE). SCOPE consists of 850-μm continuum observations of 1235 *Planck* Galactic Cold Clumps (PGCCs) made with the Submillimetre Common-User Bolometer Array 2 on the James Clerk Maxwell Telescope. These data are at an angular resolution of 14.4 arcsec, significantly improving upon the 353-GHz resolution of *Planck* at 5 arcmin, and allowing for a catalogue of 3528 compact sources in 558 PGCCs. We find that the detected PGCCs have significant substructure, with 61 per cent of detected PGCCs having 3 or more compact sources, with filamentary structure also prevalent within the sample. A detection rate of 45 per cent is found across the survey, which is 95 per cent complete to *Planck* column densities of $N_{\rm H_2} > 5 \times 10^{21}$ cm^{-2}. By positionally associating the SCOPE compact sources with YSOs, the star formation efficiency, as measured by the ratio of luminosity to mass, in nearby clouds is found to be similar to that in the more distant Galactic Plane, with the column density distributions also indistinguishable from each other.

Key words:
surveys – stars: formation – ISM: clouds – submillimetre: ISM

1 INTRODUCTION

The *Planck* survey, with its primary goal of mapping the cosmic microwave background, covered the thermal emission from dust of ∼14 K at wavelengths of 350 μm, 550 μm, and 850 μm. In the process of removing local, Galactic emission, a catalogue of 13188 *Planck* Galactic cold clumps (PGCCs) was compiled (Planck Collaboration et al. 2011a, 2016). By comparing the column densities and velocity widths of such clumps and those containing active star formation, the PGCCs were found to be significantly more quiescent and less evolved (Wu et al. 2012; Liu et al. 2013). The apparent quiescent nature of PGCCs makes them a valuable sample for studying the earliest stages of star formation, especially since they appear to have conditions suitable for star formation, with low dust temperatures of 6–20 K (Planck Collaboration et al. 2016). CO clumps have been detected towards PGCCs (e.g., Liu et al. 2013; Meng et al. 2013; Parikka et al. 2015; Zhang et al. 2016; Fehér et al. 2017), as well as detections of line emission from dense-gas tracers (Yuan et al. 2016). There can be, however, low levels of active star formation within PGCCs (Tóth et al. 2014; Liu et al. 2015; Tang et al. 2018; Yi et al. 2018; Zhang et al. 2018).

A large sample of prestellar cores and clumps needs to be studied to understand the evolution of cores and clumps after the formation of a young stellar object (YSO). In support of the effort to collect a large sample of pre- and protostellar cores and clumps, we present SCOPE, the SCUBA-2 Continuum Observations of Pre-protostellar Evolution Large Program. The project aims to test the earliest stages of star formation by observing 1235 PGCCs with the wide-field sub-mm bolometer camera, the Submillimetre Common-User Bolometer Array 2 (SCUBA-2; Holland et al. 2013) at the 850-μm wavelength beam size of 14.4 arcsec on the James Clerk Maxwell Telescope (JCMT). By observing with SCUBA-2 in the 850-μm continuum, matching the frequency of the *Planck* 353 GHz band, we can significantly improve over the 5′ resolution of the *Planck* observations of PGCCs. The 5′ resolution of *Planck* is prohibitive in that it hinders the positional cross matching of higher-resolution catalogues of YSOs (e.g Wright et al. 2010; Gutermuth & Heyer 2015; Marton et al. 2016) and also doesn't reveal the highly structured nature of the PGCCs (Juvela et al. 2012; Liu et al. 2012).

The resolution of SCUBA-2 at 850 μm resolves PGCCs at 1.5 kpc and 0.5 kpc to scales of 0.1 pc and 0.03 pc, respectively, the typical size of star-forming cores and clumps (e.g., Könyves et al. 2015), with 56 per cent and 43 per cent of sources falling within these distances, respectively (Planck Collaboration et al. 2016). It is important to resolve individual cores in the PGCCs, especially because of the close connection between the core mass spectrum and the the stellar IMF (e.g., Simpson et al. 2008; Könyves et al. 2015; Montillaud et al. 2015),

The SCOPE survey was awarded 300 hours in the JCMT weather bands 3 and 4, which correspond to sky opacity values of $\tau_{225} = 0.08$–0.2. Observations began with three periods of pilot observations occurring in September 2014, and continued from December 2015 until July 2017. SCUBA-2 does observe the 450-μm band simultaneously with the 850-μm band but the weather bands available to SCOPE do not allow for reliable photometric calibration to be made on these shorter wavelength data.

1.1 SCOPE science goals

As previously mentioned, the *Planck* survey mapped the entire sky, therefore PGCCs cover all Galactic longitudes and latitudes, from the Galactic Plane to high-latitude clouds. Previous works suggest that the Galaxy's spiral arms do not have much of an impact on star formation, other than collecting the source material together (Eden et al. 2012, 2013; Moore et al. 2012). Understanding star formation out of the Galactic Plane, however, is restricted to nearby clouds in the Gould's Belt (e.g., Ward-Thompson et al. 2007; André et al. 2010). Some clouds at higher latitudes show signs of star formation (e.g., McGehee 2008; Malinen et al. 2014; Kerp et al. 2016). Hence, high-latitude clouds could be contributing to Galactic star formation, both at present and in the future by providing source material for fresh star formation. Indeed, gas at high latitudes could be a part of a Galactic fountain, where gas and dust is expelled into the Galactic halo by supernovae and stellar winds (Bregman 1980). This material would then fall back to the Galactic Plane, cooling and condensing into atomic clouds, with observations detecting H I high-latitude clouds (Röhser et al. 2016b). These clouds then fall back onto the Plane,

⋆ E-mail: D. J. Eden@ljmu.ac.uk

replenishing the reservoir for star formation (Putman et al. 2012). In this regard, these clouds would also contain some molecular material (Magnani & Smith 2010; Röhser et al. 2016a) and dust (Planck Collaboration et al. 2011b), therefore SCOPE is important in quantifying the amount of dense gas at high latitudes and to see if it has the same star formation efficiency as in the Plane.

Images of the dust-continuum emission found that the ISM and molecular clouds are highly filamentary. with the vast majority of clumps and cores lying on, or in, these structures (Molinari et al. 2010; André et al. 2010, 2014). The formation mechanism of filaments is disputed, with global gravitational collapse (Hartmann & Burkert 2007), large-scale colliding flows in the cloud-formation process (Heitsch & Hartmann 2008), and decaying supersonic turbulence (Padoan et al. 2007) being suggested as possible formation mechanisms. Observational evidence, however, has been unable to discriminate between these possibilities. The fact that most cores, both pre- and proto-stellar, are found on these filaments implies that the filamentary structures are crucial to their formation, regardless of how the filaments form. Follow-up studies have also found PGCCs to be filamentary (e.g., Rivera-Ingraham et al. 2016; Kim et al. 2017), and the increased resolution of the SCOPE survey allows the determination of the detection rate of filaments and the fragmentation of filaments into clumps and cores. Such detection of filaments, and the placement of clumps/cores along them will allow for a greater understanding of the role that they play in star formation (Liu et al. 2018a,b; Juvela et al. 2018b).

Using the method of Sadavoy et al. (2013), we can combine *Herschel Space Observatory* data and simultaneously derive the dust temperature, column density, and dust emissivity spectral index. By calculating these values, we can study how dust properties vary between different Galactic environments and between sources in different stages of the star-formation process, with some of the sources in this study already addressed by Juvela et al. (2018a,b).

Multiple papers have already been published using the SCOPE data, namely the maps and images (Liu et al. 2016; Kim et al. 2017; Tatematsu et al. 2017; Liu et al. 2018a,b; Juvela et al. 2018a; Tang et al. 2018; Zhang et al. 2018; Yi et al. 2018; Juvela et al. 2018b).

The layout of this paper is as follows: Section 2 introduces the observing strategy and complementary observations and surveys. Section 3 describes the data and the data reduction, whilst Section 4 includes the compact source extraction. Sections 5 and 6 describe data access and results, respectively. Finally, Section 8 provides a summary and final conclusions.

2 SCOPE OBSERVING STRATEGY

The SCOPE selection of PGCCs was chosen randomly from the full PGCC sample to sample varying Galactic environments (Liu et al. 2018a). Sources from the catalogue of PGCCs were excluded if they had already been observed at the JCMT with SCUBA-2 at a rms sensitivty of at least 6 mJy beam^{-1}. These observations formed part of the JCMT Legacy Surveys (Chrysostomou 2010), namely the JCMT Plane Survey (JPS; Moore et al. 2015; Eden et al. 2017 and the JCMT Gould Belt Survey (GBS; Ward-Thompson et al. 2007). The SCUBA-2 Ambitious Sky Survey (SASSy; MacKenzie et al. 2011; Nettke et al. 2017; Thompson et al., in preparation), covers half of the Galactic Plane but does not have the desired rms.

The PGCCs not previously observed at JCMT were placed into a 3-dimensional grid with each longitude bin 30 degrees wide, latitude bins of $|b| = 0°$, 4°, 10°, and 90°, and distance bins of 0 kpc, 0.2 kpc, 0.5 kpc, 1 kpc, 2 kpc, and 8 kpc. Sources with column densities $N_{H_2} < 2 \times 10^{21}$ cm^{-2} chosen randomly within each bin, with all sources with column densities $N_{H_2} > 2 \times 10^{21}$ cm^{-2} observed. This column density criterium is due to the pilot study of the initial 300 PGCCs, where the detection rate of PGCCs with $N_{H_2} < 10^{21}$ cm^{-2} were dramatically lower. The JCMT has through SCOPE, and other archival data, covered nearly all PGCCs with column densities of $N_{H_2} > 2 \times 10^{21}$ cm^{-2} within the declination range of -30° – +35°, the most likely star-forming PGCCs (Wang et al., in preparation).

The properties of the observed sources are displayed in Fig. 1. The presented properties are Galactic longitude, Galactic latitude, temperature, distance, column density, mass, luminosity, major axis, and aspect ratio. The physical properties are not derived for all sources, and are as calculated by Planck Collaboration et al. (2016). These distributions are compared to the entire populations, as derived by Planck Collaboration et al. (2016). The biggest departure is with column density. We observed higher column density PGCCs than the average, which in turn skewed the SCOPE mass distribution to higher observed masses. Low column density ($N_{H_2} < 10^{21}$ cm^{-2}) PGCCs usually do not contain dense cores, based on our pilot observations, and thus are not interesting for star formation studies.

The average angular size of PGCCs is 8′ (Planck Collaboration et al. 2016), therefore the CV Daisy mode of SCUBA-2 was used for these observations (Bintley et al. 2014). The CV Daisy mode is specifically designed for small, compact objects, with the telescope keeping to a circular pattern at 155″ s^{-1}. Each SCOPE map takes 16 minutes to perform, with the CV Daisy mode producing 850-μm rms noise values of 6 mJy beam^{-1} in the central 3′, with 850-μm rms noise out to radii of 6′ of 10-30 mJy beam^{-1}.

The SCOPE survey including pilot studies observed fields towards 1235 PGCCs in 1062 fields, with compact source detections towards ∼ 51 per cent of fields, 45 per cent of PGCCs. The observed PGCCs in the SCOPE survey are displayed in their Galactic context in Fig. 2, with the 174 and 321 PGCCs observed by the JPS and GBS, respectively, overlaid. This paper will deal with only those observed as part of the SCOPE project.

The goal of SCOPE was to observe PGCCs in all Galactic environments. Comparison to the entire PGCC population and to sources in the GBS fields (Fig. 3) shows that SCOPE observations are representative of the high-column-density PGCC targets and complement the sources observed in GBS.

2.1 Complementary Observations

As well as the SCOPE survey, there are ongoing surveys at other facilities, giving complementary data to these PGCC detections (Liu et al. 2015, 2018a). The Taeduk Radio Astronomy Observatory (TRAO) Observations of *Planck* cold clumps (TOP) survey is observing ∼2000 PGCCs in the rotational transition of $J = 1 - 0$ of CO istopologues ^{12}CO and ^{13}CO at resolutions of 45-47 arcsec. A full description of this survey can be found in Liu et al. (2018a). Further $J = 1 - 0$ observations have been made at the Purple Mountain Observatory (PMO) at the same resolution. These observations will allow PGCCs to be put in the greater context of extended CO emission and structure.

The SMT (Submillimetre Telescope) “All-sky” Mapping of *Planck* Interstellar Nebulae in the Galaxy (SAMPLING;

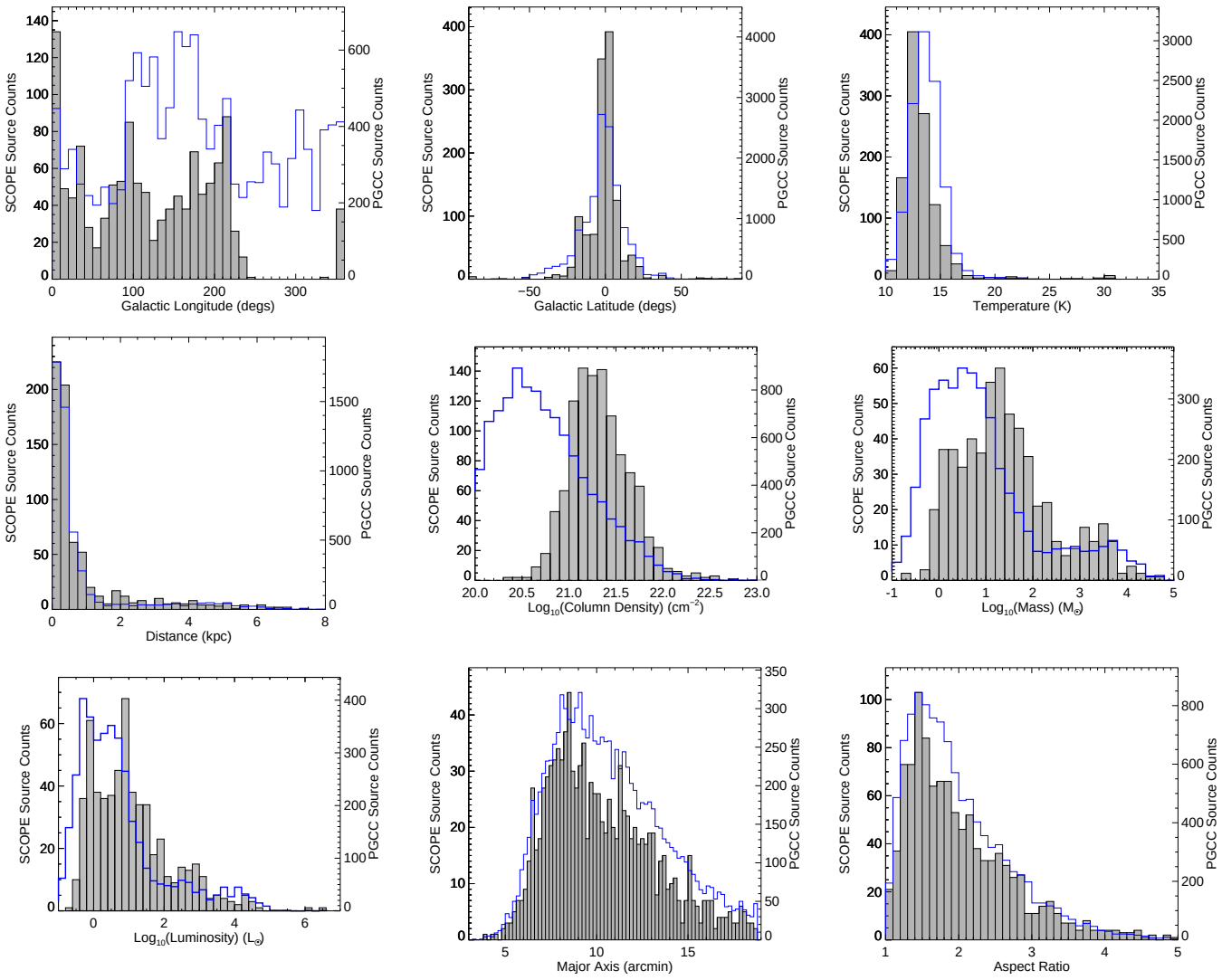

Figure 1. Properties of the PGCCs observed in the SCOPE survey (grey histogram), with the total PGCC population from Planck Collaboration et al. (2016) overlaid in blue. The top row displays the Galactic longitude, Galactic latitude, and temperature, in the left, central, and right panels, respectively. The middle row are the distance, column density, and mass, with the bottom row showing the luminosity, major axis, and aspect ratio.

Wang et al. 2018) survey follows up PGCCs in the $J = 2-1$ transition of ^{12}CO and ^{13}CO. The detection of two transitions will allow more accurate column densities to be calculated.

Further PI observations have occurred at the Nobeyama Radio Observatory 45-metre telescope, the 21-metre telescopes in Korean VLBI Network (KVN) and the Effelsberg 100-metre telescope in the dense-gas tracers like HCO^+, N_2H^+, HC_3N, CCS, DNC, $HN^{13}C$, N_2D^+ and NH_3 towards samples of SCUBA-2 dense cores in PGCCs. By observing these species, temperatures, depletion and deuteration fractions can be determined (Tatematsu et al. 2017).

3 DATA REDUCTION AND SCOPE DATA

Liu et al. (2018a) provides a full description of different data reduction methods employed and tested within the SCOPE survey.

The data reduction employed within the first SCOPE data release use the Dynamic Iterative Map-Maker (Chapin et al. 2013), part of the *Starlink* SMURF package (Jenness et al. 2011). These data make use of a 200″ spatial filter, with no use of external masking. This initial data reduction is then filtered for regions with a signal-to-noise ratio (SNR) less than 3, with these high-SNR regions used then as a mask for a further reduction. A full description of the masking process can be found in Mairs et al. (2015).

A flux conversion factor of 554 Jy beam^{-1} pW^{-1} is used to convert from the native units of pW to Jy beam^{-1}. This value is ~ 3 per cent higher than the 537 Jy beam^{-1} pW^{-1} flux conversion factor recommended by Dempsey et al. (2013b), reflecting the pixel size (4′) and data reduction method used by the SCOPE survey as the pixel size is a factor in the flux conversion factor equation.

Examples of two of the observed PGCCs are shown in Fig. 4, a complex, filamentary source, and a high-latitude cloud with simple morphology.

The mean rms within the central 12′ of the 1062 fields (this is the number of fields observed, containing the observed 1235 PGCCs) is 0.185 Jy arcsec^{-2}, which corresponds to 43.9 mJy beam^{-1}. This sensitivity is a factor of ~ 1.5 worse than the 25-31 mJy beam^{-1} rms of the JPS (Eden et al. 2017). Within

the central 3′, the rms is found to be 0.028 Jy arcsec^{-2}, which corresponds to 6.65 mJy beam^{-1}.

4 COMPACT SOURCE CATALOGUE

4.1 Compact Source Extraction

Compact sources were extracted from the images using the FELLWALKER algorithm (FW; Berry 2015)[1]. Justification for the choice of source extraction algorithm and the parameters used are outlined in Moore et al. (2015) and Eden et al. (2017). The parameter FELLWALKER:MINPIX is adjusted to account for the larger pixel size used in the SCOPE reduction.

The FW algorithm is run on the SNR maps, with the mask produced by CUPID:FINDCLUMPS used to extract flux from the emission maps.

Compact sources were initially identified in 821 of the 1062 observed fields. Sources which had a peak SNR < 5 were rejected, as well as sources with an aspect ratio > 5. The sensitivity to extended, filamentary objects in the SCOPE survey will be explored in a future study (Fich et al., in preparation). These quality control cuts resulted in 3528 sources, with examples of the source extraction results for two fields shown in Fig. 4.

Table 1 contains a portion of the full SCOPE compact source catalogue. The columns are as follows: (1) SCOPE catalogue source name; (2) SCOPE Region; (3) and (4) Right Ascension and Declination (J2000) of the peak flux position within the SCOPE source; (5) and (6) Right Ascension and Declination (J2000) of the central point; (7–9) semi-major axis, semi-minor axis, and position angle, measured anticlockwise from Equatorial north, of the ellipse fit to the shape of the SCOPE source which are not deconvolved sizes; (10) effective radius of source, calculated by $\sqrt{(A/\pi)}$, where A is the area of the source above the detection threshold of $3\sigma_{\rm rms}$; (11–12) peak flux density, in units of Jy beam^{-1}, and associated uncertainty; (13–14) integrated 850-μm flux, in units of Jy, and associated uncertainty and (15) signal-to-noise ratio (SNR) of the source, calculated from the peak flux density and the $\sigma_{\rm rms}$ from the observed field. The uncertainties take account for errors in calibration, taken to be 5 per cent (Dempsey et al. 2013b), and uncertainties in the FCF value used, also taken to be 5 per cent. A full version is included in the Supporting Information. The 3528 sources were distributed across 558 PGCCs.

The FW routine was tested extensively within the JPS survey, with a 95 per cent recovery fraction of artificial sources found to be at approximately 5σ. A full explanation can be found in Eden et al. (2017). Therefore, we are assuming that this completeness limit is valid for the observed SCOPE sources within the Galactic Plane. An improved recovery fraction of 99 per cent was found in two SCOPE fields at $|b| > 30°$.

4.2 Recovered flux densities

The FW algorithm is well understood (Eden et al. 2017). Therefore, any differences in the recovered flux densities compared to other surveys are likely due to calibration issues. To test the recovered fluxes, the SCOPE fluxes were compared to those of the JPS survey (Eden et al. 2017), both positionally matched and the survey as a whole.

The distributions of peak intensites and integrated fluxes for both surveys are displayed in Fig. 5. The JPS survey source intensities have been converted into mJy arcsec^{-2} and mJy in the peak intensity and integrated flux distributions, respectively. The peak intensity distribution of the JPS goes $\sim 2\times$ deeper than SCOPE, which corresponds to the rms values of the respective surveys. The CV Daisy mode actually produces deeper observations in the central regions, with SCOPE having greater sensitivity in those regions. The peaks of the integrated flux distributions, however, are consistent with each other. By assuming single power-law laws for the tails of the distributions of the form $\Delta N/\Delta S_\nu \propto S^{-\alpha}$, values of α for the two distributions were found to be $\alpha = 2.10 \pm 0.13$ and $\alpha = 1.97 \pm 0.10$ for the peak intensity and integrated flux distributions, respectively, above limits of 0.5 mJy arcsec^2 and 2 mJy for the peak intensity and integrated flux distributions, respectively. The SCOPE peak intensity distribution is consistent with that of the JPS ($\alpha = 2.24 \pm 0.12$) but the SCOPE integrated flux distribution is flatter than that of the JPS survey ($\alpha = 2.56 \pm 0.18$).

There is actually a slight overlap between the SCOPE and the JPS surveys. By positionally matching the two surveys within a JCMT beam of 14.4 arcsec, we find 83 matches. A comparison of peak intensities and integrated fluxes for sources in common are shown in Fig. 6. The two distributions show a slight disceprency, with the integrated fluxes departing by a greater amount. The difference between the peak fluxes can be accounted for by the difference in pixel sizes (3 arcsec in the JPS, 4 arcsec in SCOPE). As reported in Mairs et al. (2015); Rumble et al. (2015), changing the pixel size, especially to smaller sizes, can change the peak value, with 3-arcsec pixels giving the most accurate peak fluxes. The difference in integrated fluxes is accounted for by larger sources in the SCOPE survey, with sources in the SCOPE survey found to have a mean size 1.32 times that of the reported JPS source size. A linear best fit to the relationship gives a gradient of 1.06 ± 0.05. The different FCFs will also account for some of the difference. However, the major difference comes from the sensitivity in the outer edges of the SCOPE maps, where these 83 sources are found. In these regions, the JPS is $\sim 2\times$ more sensitive, thus causing the sources to be broken up in the JPS. A full explanation of this effect is contained in Eden et al. (2017) in the context of JPS and ATLASGAL (Schuller et al. 2009) comparisons.

4.3 Angular size distribution

The angular size distribution of the SCOPE sources is shown in Fig. 7. The plotted quantity is the major axis of the elliptical fit to the source, provided by FW. The reported sizes are not deconvoled sizes. The peak of the distribution, found at 35 arcsec, is in marked contrast to the peak at 8 arcmin found in the *Planck* catalogue (Planck Collaboration et al. 2016). This difference further exemplifies the inner substructure identified by the higher resolution SCOPE survey and the presence of multiple SCUBA-2 sources inside a single PGCC, which is highlighted in Fig. 8, where 61 per cent of detected PGCCs have 3 or more SCOPE sources.

We present the aspect ratios of the SCOPE sources in Fig. 9. We have overlaid the aspect ratios of the observed *Planck* PGCCs in this survey. Planck Collaboration et al. (2016) found that 40 per cent of sources had an aspect ratio of between 2 and 3, with a shoulder at those values not present in the SCOPE compact source catalogue. This shoulder in the PGCC catalogue aspect ratios is a hint at the substructure observed by SCOPE, with a higher aspect ratio pointing towards more filamentary structures. It is also a reflection of the nature of the sources extracted by the FW algorithm, which is attuned more towards extracting compact objects.

[1] FW is part of the *Starlink* CUPID package outlined in Berry et al. (2007).

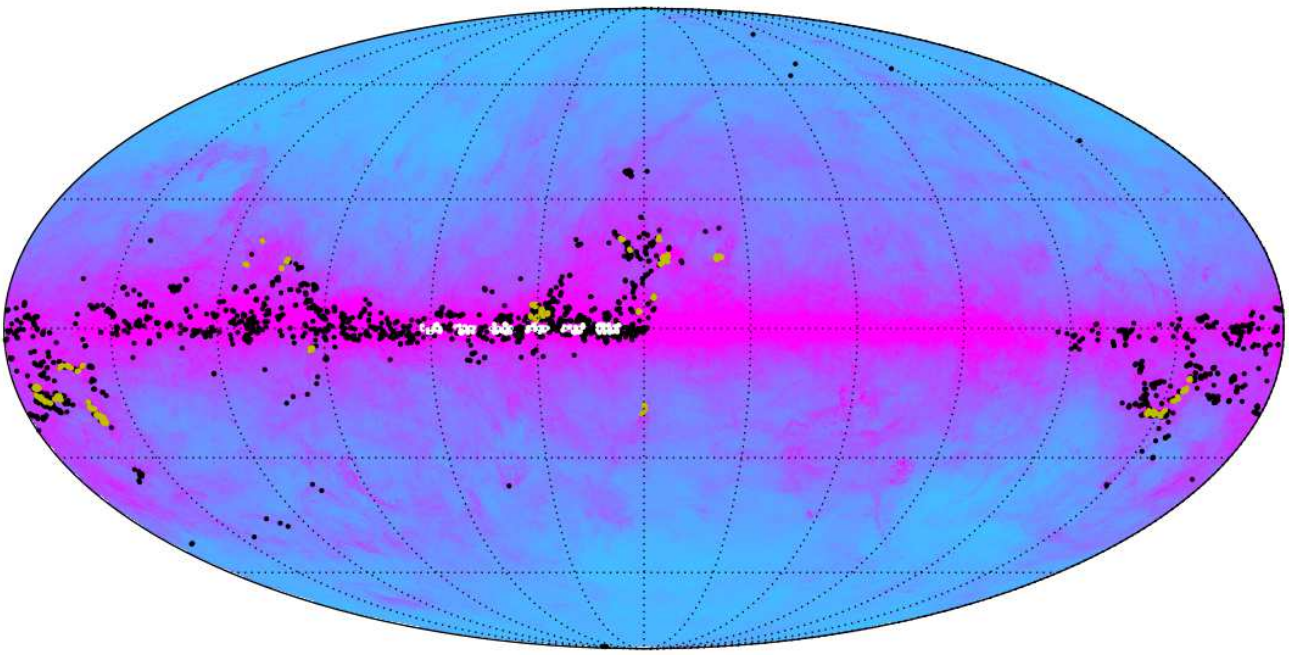

Figure 2. The distribution of observed PGCCs by the JCMT. The black points represent SCOPE sources, whilst the white and gold points were observed as part of the JPS and GBS, respectively. The underlying image is the *Planck* 353-GHz (850-μm) intensity map.

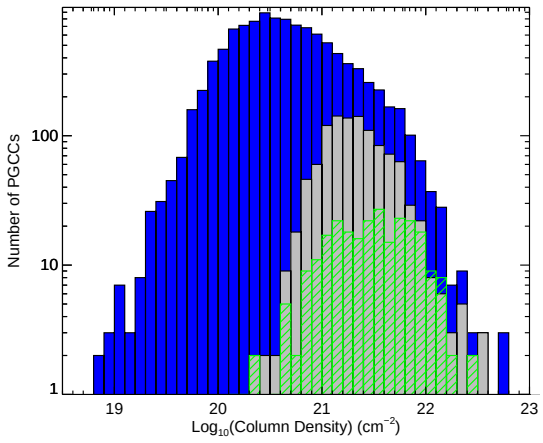

Figure 3. Histograms of column density of PGCCs with the entire population represented by the blue histogram, the grey histogram representing those PGCCs observed by SCOPE and the green hashed histogram covering those PGCCs observed by the JCMT in the Gould's Belt Survey ((Ward-Thompson et al. 2007).

5 SCOPE SURVEY AND DATA ACCESS

The SCOPE data products can be downloaded from the Canadian Astronomy Data Centre's JCMT Science Archive[2], with the proposal IDs MJLSY14B, M15AI05, M15BI06, and M16AL003. These IDs correspond to observations taken in the SASSy survey, two PI proposals, all of which formed the pilot observations, and the SCOPE survey, respectively. As well as these data, the raw observation data can also be downloaded from the same location.

The full source compact source catalogue is available as Supporting Information.

6 RESULTS

6.1 Detection statistics

The PGCCs observed in the SCOPE survey were chosen to sample across the spectrum of a host of statistics, as displayed in Fig.1, with a bias towards the highest column density sources, as described earlier. The detection rate of each statistic is shown in Fig.10. Six high-latitude PGCCs with detections ($|b| > 30°$) were

[2] http://www.cadc-ccda.hia-iha.nrc-cnrc.gc.ca/en/jcmt/

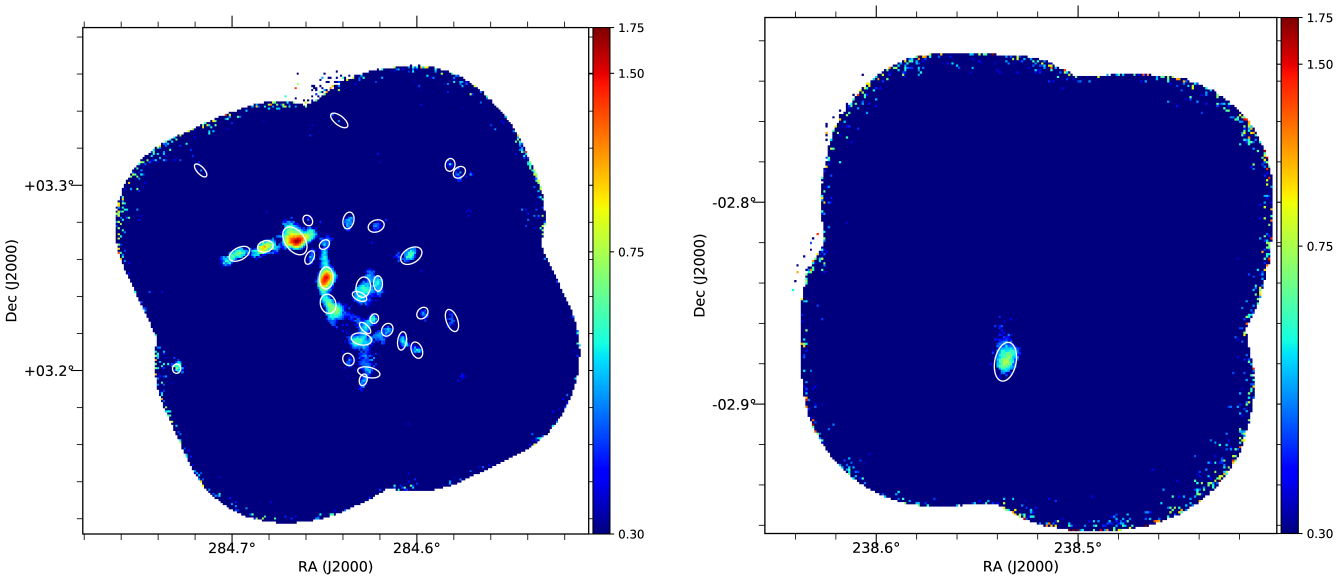

Figure 4. Examples of observed PGCCs in the SCOPE survey. Left panel: A complicated, filamentary source at Galactic coordinates $\ell = 36.^{\circ}62$, $b = -0.^{\circ}11$, PGCC_G36.62-0.11. Right panel: A high-latitude PGCC, positioned at $\ell = 6.^{\circ}04$, $b = 36.^{\circ}77$, PGCC_G6.04+36.77 (Liu et al., in preparation). The intensity scale in each image is mJy arcsec^{-2} and the white ellipses represent the elliptical fits to the FELLWALKER extractions within the observed field.

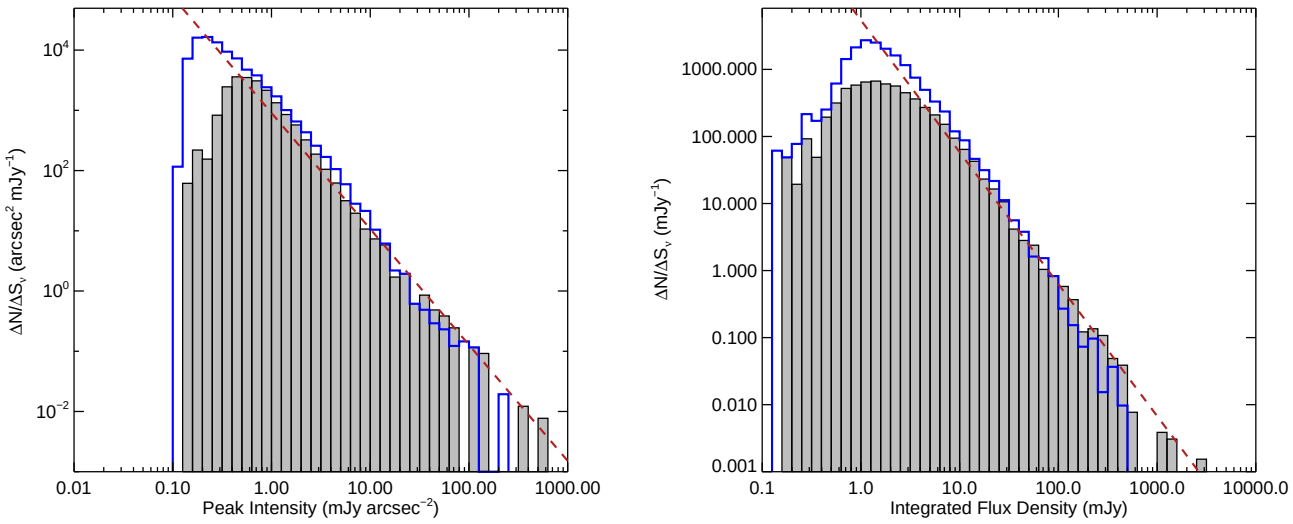

Figure 5. Peak and integrated flux distributions for the SCOPE survey (grey, filled histogram) compared to the JPS (blue histogram) in the left and right panels, respectively. The least-squares fit to the SCOPE distributions are indicated by the red, dashed line.

excluded from the statistics as they were found to be associated with lensed galaxies (Liu et al., in preparation).

The longitude detection rates are approximately equal to the overall detection rate (0.46), with lower rates found in the central 20 degrees ($|b| < 2^{\circ}$). In these longitudes, higher latitude sources are observed, with lower detection rates found outside of the central 4 degrees ($|b| > 2^{\circ}$) of the Galactic Plane. In the latitude range of $|b| < 2^{\circ}$, the detection rate is slightly higher than the overall rate, approximately 0.50. This is also reflected in the detection rate as a function of distance. The detection rate at higher distances, those classically taken to be in the Galactic Plane, are well detected. However, the local, higher latitude sources are not detected at as higher rate.

The column densities are 95 per cent complete above densities of $N_{\mathrm{H_2}} > 5 \times 10^{21}$ cm^{-2}. This detection rate corresponds to the threshold for star formation found in studies of nearby star-forming clouds (André et al. 2010; Heiderman et al. 2010; Lada et al. 2010; André et al. 2014) Some bins are subject to low detection rates due to low number statistics. The mass and lumniosities are complete to a 95 per cent rate above 5×10^3 M$_\odot$ and 1×10^3 L$_\odot$, respectively.

The column density detection rate does not account for the selection bias imposed on the initial sample. When comparing the entire PGCC population, the observed SCOPE sample, and the detected PGCCs in SCOPE, we can see that the highest column density sources are confined to the lower latitudes, which are the

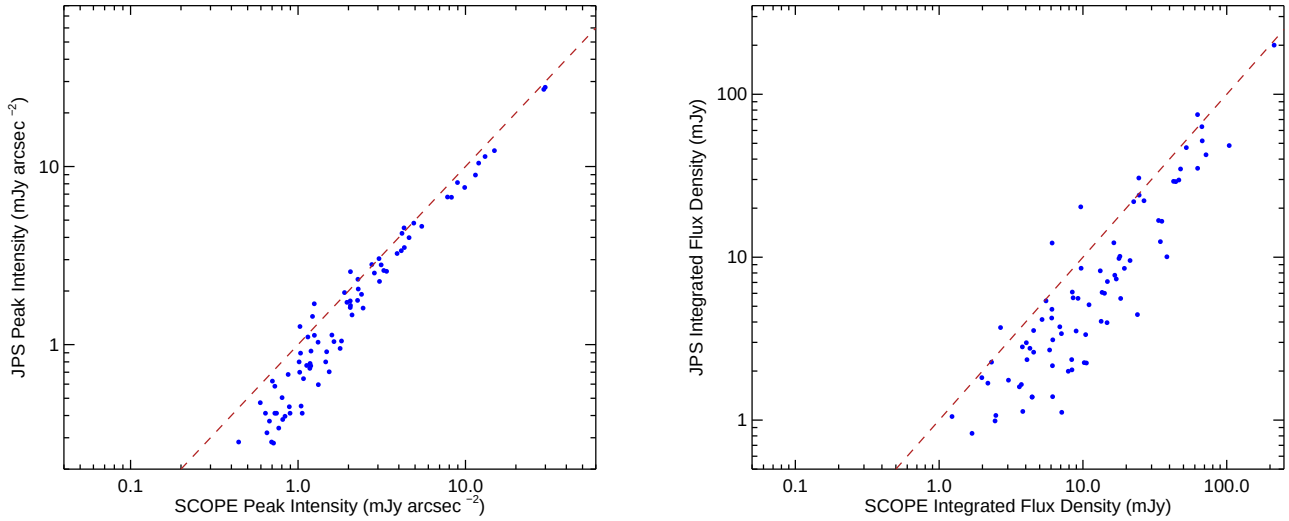

Figure 6. Comparison of the recovered peak and total fluxes for positionally matched SCOPE and JPS sources, in the left and right panels, respectively. The red dashed line represents the 1:1 line.

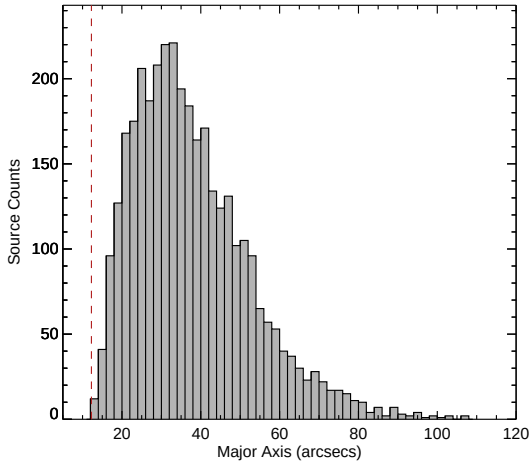

Figure 7. Histogram of the major axes identified by FELLWALKER of the extracted SCOPE compact sources. The red dashed line indicates the beam size of the JCMT at 850 μm.

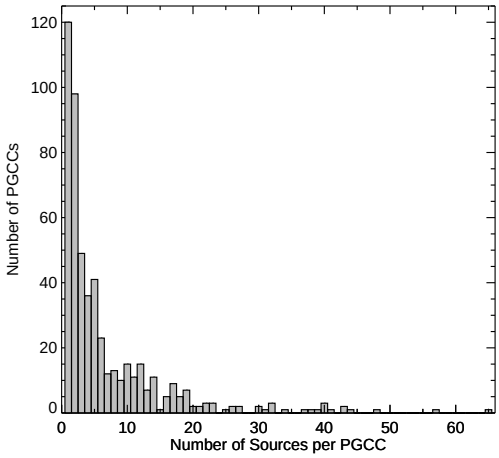

Figure 8. Histogram of the number of compact sources extracted per PGCC with a detection in the SCOPE survey.

PGCCs with the largest distances, as seen in Fig. 11. Deeper observations will be required to trace the lowest column density objects.

The major axes and aspect ratios fluctuate around the actual detection rate of the SCOPE survey.

The detection rate of the temperatures is skewed by the lack of derived temperatures by Planck Collaboration et al. (2016). 619 of the 1235 observed PGCCs do not have derived temperatures, with 360 of those 619 detected in SCOPE. The detection rate at the lower temperatures of less than 15 K is 0.15.

6.2 Star formation out of the Galactic Plane

The SCOPE survey gives a sample of potentially star-forming cores and clumps in different Galactic environments. The YSO catalogue of Marton et al. (2016) provides an all-sky catalogue derived from the AllWISE catalogue (Cutri et al. 2013). By positionally matching these two catalogues, we find 865 YSOs located within the map extents of 201 observed PGCCs that have detected compact sources.

The YSO catalogue of Marton et al. (2016) contains the magnitudes of the 4 WISE bands (3.4 μm, 4.6 μm, 12 μm, and 22 μm) as well as the *J*, *H*, and *K* bands from the positional matching of 2MASS Point Sources (Cutri et al. 2003). These 7 bands can be used to calculate the luminosities of each YSO, and therefore the total YSO luminosity associated with a PGCC. The luminosities are calculated, once the magnitudes are converted into fluxes, using a trapezium rule estimation in log-log space, which was shown to provide a good approximation of the luminosity (Eden et al. 2015), with other studies using this method (e.g., Veneziani et al. 2013).

These luminosities, L, can be compared to the masses, M, of the SCOPE detected YSOs to determine the ratio of L/M, a measure of the current star formation and an indicator of the evolutionary state of that star formation (e.g., Elia et al. 2017; Urquhart et al. 2018). Comparing this ratio between the nearby sources, complementary to the Gould's Belt, and the more distant Galactic Plane

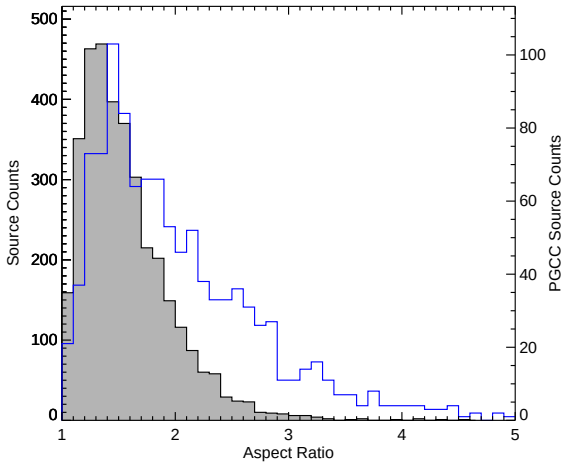

Figure 9. Histogram of the aspect ratios of all SCOPE sources (grey histogram) with the aspect ratios of the SCOPE-observed PGCCs overlaid in the blue histogram.

can determine whether the star formation in either environment is at a different evolutionary stage (on average).

The masses were derived from the total emission within the SCOPE maps. The masses in the SCOPE maps are estimated using the optically thin approximation:

$$M = \frac{S_\nu D^2}{\kappa_\nu B_\nu(T_d)} \quad (1)$$

where S_ν is the integrated flux of the emission, D is the distance (omitted in the calculation for the ratio of L/M), κ_ν is the mass absorption coefficient taken to be 0.01 $\mathrm{cm^2\,g^{-1}}$ (Mitchell et al. 2001) which accounts for a gas-to-dust ratio of 100, and $B_\nu(T_d)$ is the Planck function evaluated at temperature, T_d, taken to be 13 K, the peak of the SCOPE-observed PGCC-temperature distribution.

The sample of 201 PGCCs with a YSO was split into two populations, a Gould's Belt-like population and the distant Galactic Plane. This was done by using a distance cut of 0.5 kpc, as this is taken to be the furthest Gould's Belt sources (Ward-Thompson et al. 2007), with distances below this in the Gould's Belt, and greater distances in the Galactic Plane. From hereafter, these populations will be referred to as the nearby and distant samples, respectively. The distances were estimated in three ways. The first was to take the distances as derived by Planck Collaboration et al. (2016). This accounted for 91 PGCCs. The second was to extract spectra from spectral line data from existing surveys (Dame et al. 2001; Jackson et al. 2006; Dempsey et al. 2013a; Rigby et al. 2016), with sources in the Plane compared to the Galactic rotation curve of Brand & Blitz (1993). This accounted for a further 108 PGCCs. The final two were well out of the Plane at high latitudes, and were assumed to be local.

We found 114 and 87 PGCCs in the distant and nearby samples, respectively. The distribution of the L/M ratios for each of these populations is shown in Fig. 12. The mean values of the two populations are $0.78 \pm 0.16\,\mathrm{L_\odot/M_\odot}$ and $1.14 \pm 0.30\,\mathrm{L_\odot/M_\odot}$ for the distant and nearby samples, respectively, with median values of $0.21 \pm 0.16\,\mathrm{L_\odot/M_\odot}$ and $0.32 \pm 0.28\,\mathrm{L_\odot/M_\odot}$, respectively. The populations are consistent with each other, within the errors, indicating that the star formation in the distant Galactic Plane is at roughly the same evolutionary stage as that within the nearby Gould's Belt-like sample. A Kolomogorov–Smirnov (K–S) test of the two subsamples finds a 25 per cent chance they are not drawn from the same distribution. We therefore cannot strongly reject the null hypothesis that they are not drawn from the same sample and that the distributions at different distances are different. The sample of the Galactic Plane PGCCs will be extended when JPS sources are also included, and this analysis will be the subject of a further study (Eden et al., in preparation).

6.3 Column densities of SCOPE sources

The column densities of the SCOPE sources in the nearby environments and the distant Galactic Plane are compared. The column densities were calculated using the following:

$$N_{\mathrm{H_2}} = \frac{S_{\nu,\mathrm{peak}}}{B_\nu(T_d)\Omega_\mathrm{b}\kappa_\nu m_\mathrm{H}\mu} \quad (2)$$

where $S_{\nu,\mathrm{peak}}$ is the peak intensity, $B_\nu(T_d)$ and κ_ν are as defined above, Ω_b is the solid angle of the beam, m_H is the mass of a hydrogen atom, and μ is the mean mass per hydrogen molecule, taken to be 2.8 (Kauffmann et al. 2008).

The distribution of column densities for the entire SCOPE sample, as well as the two subsamples are displayed in Fig. 13 (top, middle), with the cumulative distribution also included. A K–S test of the two subsamples gives a $\sim 2.5\,\sigma$, or a 2.5 per cent chance that they are not drawn from the same population. We therefore cannot strongly reject the null hypothesis that they are not drawn from the same sample.

When comparing only the star-forming samples, as shown in Fig.13 (bottom), the K–S test gives a 94 per cent result that the nearby and distant Galactic Plane SCOPE sources are drawn from the same population. We can assume, however, that the total star-forming sample is considerably different from the entire SCOPE sample due to a K-S test giving a probability of their being the same of 0.001. This result is consistent with that of Urquhart et al. (2014), who found that the star-forming clumps in the ATLASGAL survey had a considerably different column-density distribution than that of the entire population.

7 SUMMARY

We present the first data release of the SCOPE survey, presenting the data images and a compact source catalogue. The data consist of observations of 1235 *Planck* Galactic Cold Clumps (PGCCs) at angular resolutions of 14.4 arcsec, significantly improving upon the 5-arcmin resolution of *Planck*. The improved resolution reveals significant substructure within these sources, reflected by a compact source catalogue consisting of 3528 sources. The data are downloadable from the CADC, with the compact source catalogue included as Supporting Information to this article.

The compact source catalogue was produced using the FELLWALKER algorithm, reflecting the same method used within the JCMT Plane Survey (JPS; Eden et al. 2017). A comparison of peak intensities and integrated fluxes in overlapping sources between the JPS and SCOPE surveys shows slight discrepancies, but otherwise good agreement. The SCOPE sources are significantly smaller than those within the *Planck* catalogue, with peaks of the angular-size distribution found at 35 arcsec compared to 8 arcmin.

The detection rate of PGCCs within the SCOPE survey is 45 per cent, with 558 PGCCs detected of the 1235 observed. The survey is 95 complete in PGCCs with column den-

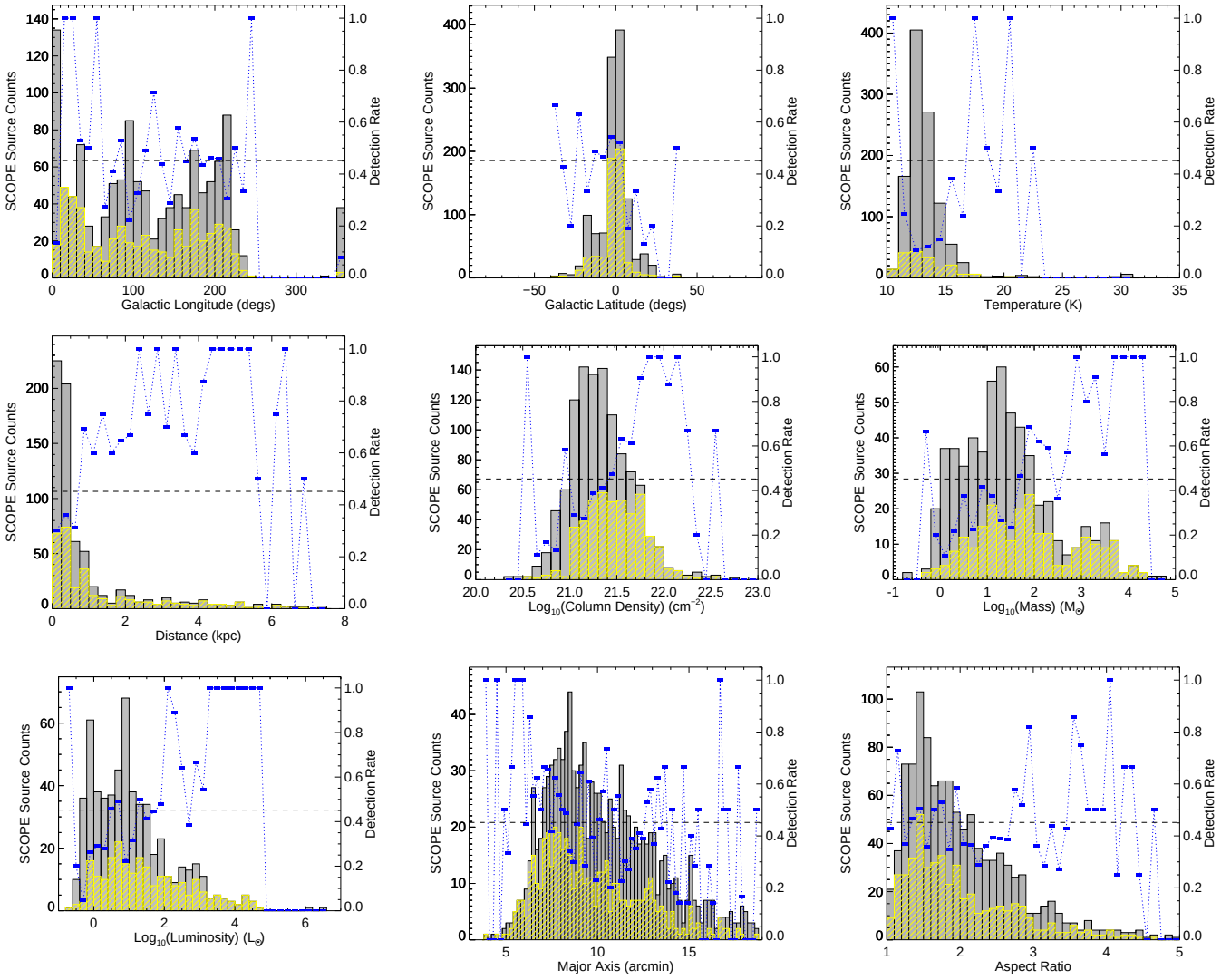

Figure 10. Distributions of the observed, *Planck*-derived statistics of SCOPE sources (grey histograms) overlaid with the detected PGCCs (yellow hashed histogram). The ratio of the two histograms is overlaid by the blue dotted line. The black dashed line respresents the overall detection rate. As in Fig. 1, the top row displays the Galactic longitude, Galactic latitude, and temperature, in the left, central, and right panels, respectively. The middle row are the distance, column density, and mass, with the bottom row showing the luminosity, major axis, and aspect ratio.

sities $N_{\mathrm{H_2}} > 5 \times 10^{21}\,\mathrm{cm^{-2}}$, and to masses and luminosities of $5 \times 10^3\,\mathrm{M_\odot}$ and $1 \times 10^3\,\mathrm{L_\odot}$, respectively.

By positionally matching the SCOPE compact sources with YSOs from the WISE catalogue, and splitting the sample into sources that are within 0.5 kpc and those at greater distances, we found that the ratio of L/M is consistent between these samples. The column densities of these two samples of SCOPE sources are also consistent. The distribution of column densities of star-forming sources, however, were found to be significantly different from those of the whole SCOPE compact source catalogue.

ACKNOWLEDGEMENTS

The authors would like to thank the anonymous referee for their comments, they have greatly improved the quality of the paper. DJE is supported by a STFC postdoctoral grant (ST/M000966/1). MJ acknowledges the support of the Academy of Finland Grant No. 285769. DC is currently supported by the Centre National d'Études Spatiales (CNES) through PhD grant 0102541 and the Région Bourgogne Franche-Comté. MK was supported by Basic Science Research Program through the National Research Foundation of Korea (NRF) funded by the Ministry of Science, ICT & Future Planning (No. NRF-2015R1C1A1A01052160). CWL is supported by Basic Science Research Program through the National Research Foundation of Korea (NRF) funded by the Ministry of Education, Science and Technology (NRF-2016R1A2B4012593). JHH is supported by the NSF of China under Grant Nos. 11873086 and U1631237, partly by Yunnan province (2017HC018), and also partly by the Chinese Academy of Sciences (CAS) through a grant to the CAS South America Center for Astronomy (CASSACA) in Santiago, Chile. The James Clerk Maxwell Telescope is operated by the East Asian Observatory on behalf of The National Astronomical Observatory of Japan; Academia Sinica Institute of Astronomy and Astrophysics; the Korea Astronomy and Space Science Institute; the Operation, Maintenance and Upgrading Fund for

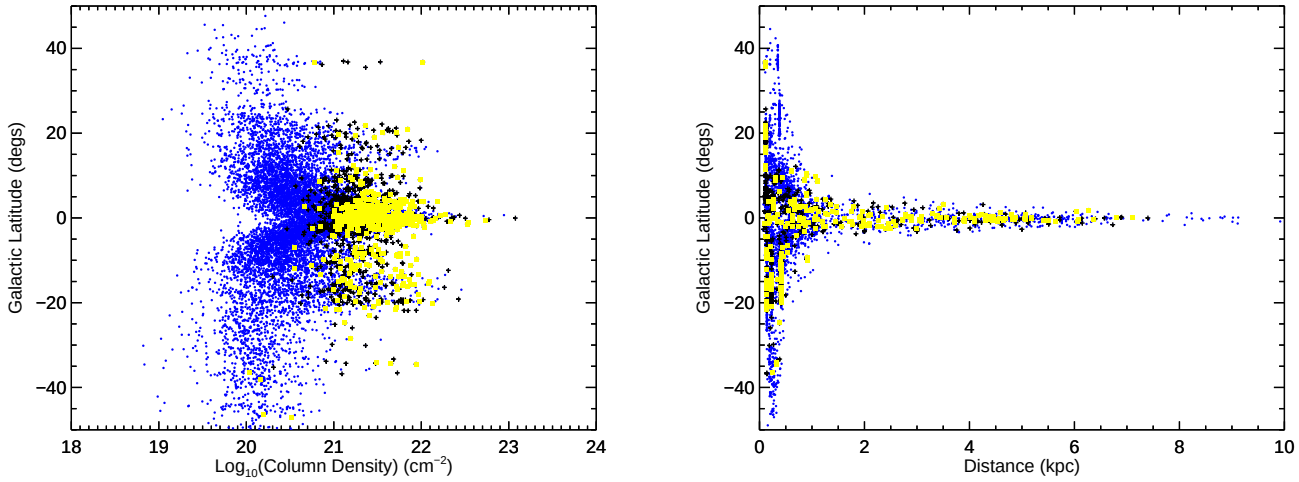

Figure 11. Latitude of PGCCs against column density (left panel) and distance (right panel). The blue circles are the entire PGCC sample from Planck Collaboration et al. (2016), the black plus symbols are the observed SCOPE PGCCs, with the yellow squares representing the detected SCOPE PGCCs.

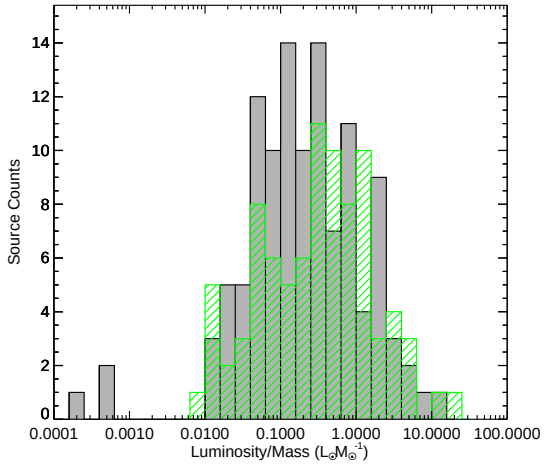

Figure 12. Histogram of the L/M ratios in SCOPE detected PGCCs in the further (grey) and in the nearby (green) Galactic Plane.

Astronomical Telescopes and Facility Instruments, budgeted from the Ministry of Finance (MOF) of China and administrated by the Chinese Academy of Sciences (CAS), as well as the National Key R&D Program of China (No. 2017YFA0402700). Additional funding support is provided by the Science and Technology Facilities Council of the United Kingdom and participating universities in the United Kingdom and Canada. The JCMT has historically been operated by the Joint Astronomy Centre on behalf of the Science and Technology Facilities Council of the United Kingdom, the National Research Council of Canada and the Netherlands Organization for Scientific Research. Additional funds for the construction of SCUBA-2 were provided by the Canada Foundation for Innovation. This research was carried out in part at the Jet Propulsion Laboratory which is operated for NASA by the California Institute of Technology. This research has made use of NASA's Astrophysics Data System. The Starlink software (Currie et al. 2014) is currently supported by the East Asian Observatory. DJE would like to dedicate this work to his auntie, Marjorie Eden.

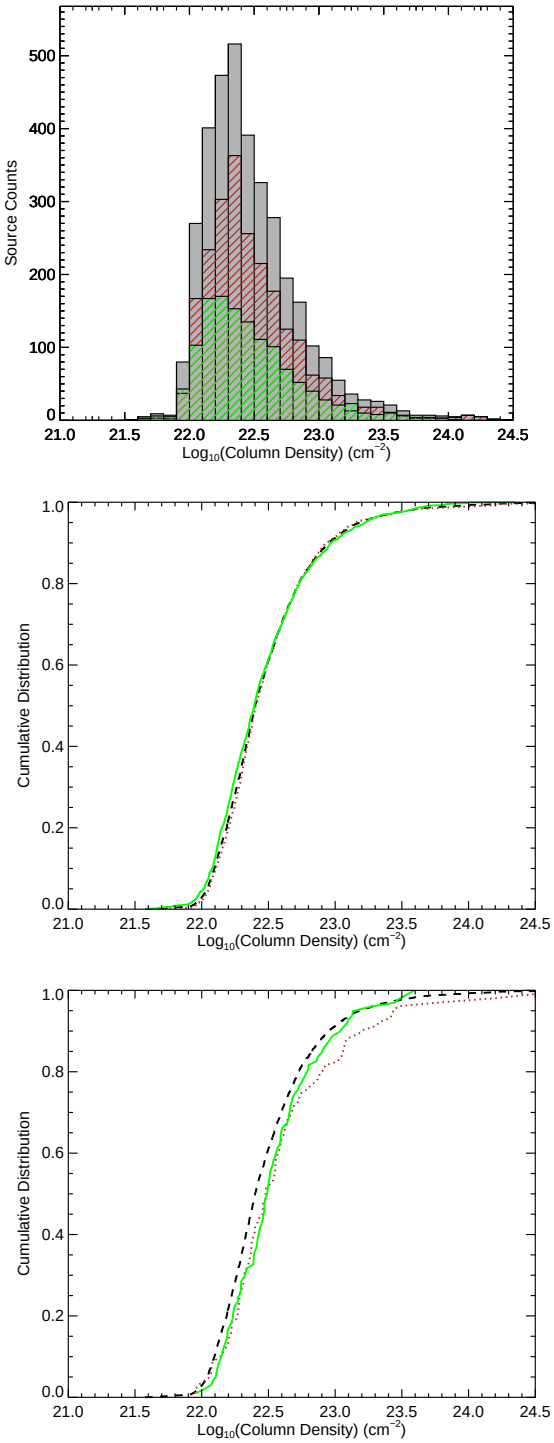

Figure 13. Top panel: column density distribution of all SCOPE compact sources (grey histogram), with those in the distant Galactic Plane ($d > 500$ pc; red histogram) and nearby sample ($d < 500$ pc; green histogram). Middle panel: the cumulative distributions of the same histograms with the dashed black line, dotted red line, and green solid line representing, the whole sample, in the distant Galactic Plane and nearby Plane, respectively. Bottom panel: the cumulative distributions of the star-forming samples, with the dashed black line representing the total sample (as in the middle panel, includes non-star-forming sources), and the dotted red lines and green solid lines represent the star-forming sources in distant and nearby environments, respectively.

Table 1. The SCOPE compact source catalogue. The columns are as defined in Section 4.1.

Name	Region	RA_{peak}	Dec_{peak}	RA_{cen}	Dec_{cen}	σ_{maj}	σ_{min}	PA	R_{eff}	S_{peak}	ΔS_{peak}	S_{int}	ΔS_{int}	SNR
		(°)	(°)	(°)	(°)	(″)	(″)	(°)	(″)	(Jy arcsec^{-2})	(Jy arcsec^{-2})	(Jy)	(Jy)	
(1)	(2)	(3)	(4)	(5)	(6)	(7)	(8)	(9)	(10)	(11)	(12)	(13)	(14)	(15)
SCOPEG000.39+11.38	G0.49+11.38a	256.139	-22.294	256.139	-22.299	15	7	260	20	0.308	0.035	0.647	0.032	5.39
SCOPEG000.41+11.41	G0.49+11.38a	256.120	-22.259	256.115	-22.258	17	11	207	29	0.943	0.025	4.232	0.212	16.53
SCOPEG001.37+20.94	G001.3+20.9A1	248.655	-15.791	248.660	-15.794	23	15	192	43	1.132	0.151	7.936	0.397	11.26
SCOPEG001.37+20.95	G001.3+20.9A1	248.647	-15.782	248.647	-15.781	21	18	132	46	1.379	0.202	14.625	0.731	13.71
SCOPEG001.37+20.96	G001.3+20.9A1	248.636	-15.776	248.634	-15.771	18	14	222	33	1.038	0.155	4.771	0.239	10.33
SCOPEG001.82+16.56	G001.8+16.5A1	252.559	-18.105	252.559	-18.104	24	15	190	42	0.651	0.081	4.494	0.225	7.82
SCOPEG003.98+35.70	G4.18+35.79a	238.346	-4.808	238.357	-4.798	37	20	162	58	3.143	0.050	42.604	2.130	24.61
SCOPEG004.00+35.71	G4.18+35.79a	238.350	-4.788	238.356	-4.778	48	33	167	79	1.515	0.081	35.849	1.792	11.86
SCOPEG004.01+35.66	G4.18+35.79a	238.394	-4.809	238.390	-4.806	13	8	161	21	3.071	0.050	7.201	0.360	24.04
SCOPEG004.02+35.66	G4.18+35.79a	238.398	-4.808	238.400	-4.801	15	10	140	26	2.137	0.027	6.655	0.333	16.73
SCOPEG004.61+36.64	G004.5+36.7A1	237.928	-3.821	237.918	-3.837	45	21	115	68	15.535	0.069	243.776	12.189	27.44
SCOPEG004.62+36.64	G004.5+36.7A1	237.927	-3.816	237.918	-3.817	29	8	156	37	13.091	0.062	68.204	3.410	23.12
SCOPEG004.62+36.65	G004.5+36.7A1	237.926	-3.810	237.914	-3.799	40	20	254	66	12.707	0.049	167.376	8.369	22.44
SCOPEG005.00+18.99	G005.0+19.0A1	252.391	-14.230	252.389	-14.229	9	4	143	11	1.117	0.026	0.755	0.038	17.61
SCOPEG005.23-01.99	G5.17-1.97	271.305	-25.426	271.305	-25.427	14	10	195	26	0.724	0.077	2.136	0.107	7.34
SCOPEG005.64+00.23	G5.73+0.19	269.408	-23.968	269.411	-23.972	22	13	219	36	1.930	0.147	9.894	0.495	10.58
SCOPEG005.64+00.24	G5.73+0.19	269.395	-23.966	269.394	-23.962	25	17	239	51	12.946	0.153	62.862	3.143	71.00
SCOPEG005.65+00.22	G5.73+0.19	269.416	-23.964	269.416	-23.960	28	14	254	47	1.665	0.225	10.648	0.532	9.13
SCOPEG005.65+00.26	G5.73+0.19	269.381	-23.944	269.380	-23.944	8	6	123	14	0.917	0.050	1.119	0.056	5.03
SCOPEG005.83−00.94	G005.91−01.00	270.615	-24.383	270.618	-24.382	15	9	227	26	1.654	0.050	5.157	0.258	12.63
SCOPEG005.83−01.03	G005.91−01.00	270.704	-24.435	270.703	-24.443	31	14	97	35	0.788	0.040	3.053	0.153	6.02
SCOPEG005.84−01.00	G005.91−01.00	270.676	-24.406	270.678	-24.412	32	24	267	65	2.297	0.246	22.732	1.137	17.54
SCOPEG005.85−00.99	G005.91−01.00	270.682	-24.392	270.683	-24.390	15	15	102	35	1.618	0.254	8.175	0.409	12.35
SCOPEG005.85−01.00	G005.91−01.00	270.693	-24.397	270.697	-24.399	18	14	204	32	0.753	0.105	3.974	0.199	5.75
SCOPEG005.87−00.99	G005.91−01.00	270.693	-24.375	270.693	-24.378	28	12	243	40	1.183	0.164	8.784	0.439	9.03
SCOPEG005.88−00.94	G005.91−01.00	270.648	-24.345	270.645	-24.352	27	25	109	58	0.999	0.138	15.217	0.761	7.62
SCOPEG005.88−01.01	G005.91−01.00	270.709	-24.374	270.705	-24.372	22	13	257	38	2.814	0.397	14.790	0.739	21.49
SCOPEG005.89−00.91	G005.91−01.00	270.624	-24.325	270.629	-24.320	23	14	161	39	0.723	0.091	5.750	0.287	5.52
SCOPEG005.89−00.94	G005.91−01.00	270.656	-24.334	270.655	-24.331	15	12	240	32	1.727	0.193	5.672	0.284	13.18
SCOPEG005.90−00.93	G005.91−01.00	270.650	-24.317	270.648	-24.315	16	10	234	31	1.162	0.123	4.413	0.221	8.88
SCOPEG005.90−01.01	G005.91−01.00	270.721	-24.362	270.720	-24.371	46	24	261	72	1.936	0.248	36.472	1.824	14.78
SCOPEG005.91−00.95	G005.91−01.00	270.675	-24.318	270.671	-24.319	25	18	256	51	2.880	0.294	14.736	0.737	21.99
SCOPEG005.91−01.00	G005.91−01.00	270.724	-24.345	270.725	-24.344	20	10	141	30	1.467	0.354	9.249	0.462	11.20
SCOPEG005.91−01.02	G005.91−01.00	270.742	-24.357	270.740	-24.354	23	21	223	54	2.246	0.442	20.771	1.039	17.15
SCOPEG005.92−00.96	G005.91−01.00	270.683	-24.313	270.683	-24.311	12	9	117	22	0.722	0.121	1.833	0.092	5.51
SCOPEG005.92−00.97	G005.91−01.00	270.696	-24.317	270.696	-24.316	13	12	170	29	0.695	0.138	2.919	0.146	5.31
SCOPEG005.92−00.99	G005.91−01.00	270.714	-24.335	270.713	-24.335	31	23	156	62	2.432	0.550	27.790	1.389	18.57
SCOPEG005.96−01.12	G005.91−01.00	270.857	-24.359	270.843	-24.361	23	15	162	36	0.701	0.032	4.665	0.233	5.35

Note: Only a small portion of the catalogue is shown here. The entire catalogue is available in the Supporting Information.

REFERENCES

André P., et al., 2010, A&A, 518, L102
André P., Di Francesco J., Ward-Thompson D., Inutsuka S.-I., Pudritz R. E., Pineda J. E., 2014, Protostars and Planets VI, pp 27–51
Berry D. S., 2015, Astronomy and Computing, 10, 22
Berry D. S., Reinhold K., Jenness T., Economou F., 2007, in Shaw R. A., Hill F., Bell D. J., eds, Astronomical Society of the Pacific Conference Series Vol. 376, Astronomical Data Analysis Software and Systems XVI. p. 425
Bintley D., et al., 2014, in Millimeter, Submillimeter, and Far-Infrared Detectors and Instrumentation for Astronomy VII. p. 915303, doi:10.1117/12.2055231
Brand J., Blitz L., 1993, A&A, 275, 67
Bregman J. N., 1980, ApJ, 236, 577
Chapin E. L., Berry D. S., Gibb A. G., Jenness T., Scott D., Tilanus R. P. J., Economou F., Holland W. S., 2013, MNRAS, 430, 2545
Chrysostomou A., 2010, Highlights of Astronomy, 15, 797
Currie M. J., Berry D. S., Jenness T., Gibb A. G., Bell G. S., Draper P. W., 2014, in Manset N., Forshay P., eds, Astronomical Society of the Pacific Conference Series Vol. 485, Astronomical Data Analysis Software and Systems XXIII. p. 391
Cutri R. M., et al., 2003, 2MASS All Sky Catalog of point sources.
Cutri R. M., et al., 2013, VizieR Online Data Catalog, 2328
Dame T. M., Hartmann D., Thaddeus P., 2001, ApJ, 547, 792
Dempsey J. T., Thomas H. S., Currie M. J., 2013a, ApJS, 209, 8
Dempsey J. T., et al., 2013b, MNRAS, 430, 2534
Eden D. J., Moore T. J. T., Plume R., Morgan L. K., 2012, MNRAS, 422, 3178
Eden D. J., Moore T. J. T., Morgan L. K., Thompson M. A., Urquhart J. S., 2013, MNRAS, 431, 1587
Eden D. J., Moore T. J. T., Urquhart J. S., Elia D., Plume R., Rigby A. J., Thompson M. A., 2015, MNRAS, 452, 289
Eden D. J., et al., 2017, MNRAS, 469, 2163
Elia D., et al., 2017, MNRAS, 471, 100
Fehér O., Juvela M., Lunttila T., Montillaud J., Ristorcelli I., Zahorecz S., Tóth L. V., 2017, A&A, 606, A102
Gutermuth R. A., Heyer M., 2015, AJ, 149, 64
Hartmann L., Burkert A., 2007, ApJ, 654, 988
Heiderman A., Evans II N. J., Allen L. E., Huard T., Heyer M., 2010, ApJ, 723, 1019
Heitsch F., Hartmann L., 2008, ApJ, 689, 290
Holland W. S., et al., 2013, MNRAS, 430, 2513
Jackson J. M., et al., 2006, ApJS, 163, 145
Jenness T., Berry D., Chapin E., Economou F., Gibb A., Scott D., 2011, in Evans I. N., Accomazzi A., Mink D. J., Rots A. H., eds, Astronomical Society of the Pacific Conference Series Vol. 442, Astronomical Data Analysis Software and Systems XX. p. 281 (arXiv:1011.5876)
Juvela M., et al., 2012, A&A, 541, A12
Juvela M., et al., 2018a, A&A, 612, A71
Juvela M., et al., 2018b, A&A, 620, A26
Kauffmann J., Bertoldi F., Bourke T. L., Evans II N. J., Lee C. W., 2008, A&A, 487, 993
Kerp J., Lenz D., Röhser T., 2016, A&A, 589, A123
Kim J., et al., 2017, ApJS, 231, 9
Könyves V., et al., 2015, A&A, 584, A91
Lada C. J., Lombardi M., Alves J. F., 2010, ApJ, 724, 687
Liu T., Wu Y., Zhang H., 2012, ApJS, 202, 4
Liu T., Wu Y., Zhang H., 2013, ApJ, 775, L2
Liu T., et al., 2015, Publication of Korean Astronomical Society, 30, 79
Liu T., et al., 2016, ApJS, 222, 7
Liu T., et al., 2018a, ApJS, 234, 28
Liu T., et al., 2018b, ApJ, 859, 151
MacKenzie T., et al., 2011, MNRAS, 415, 1950
Magnani L., Smith A. J., 2010, ApJ, 722, 1685
Mairs S., et al., 2015, MNRAS, 454, 2557
Malinen J., et al., 2014, A&A, 563, A125
Marton G., Tóth L. V., Paladini R., Kun M., Zahorecz S., McGehee P., Kiss C., 2016, MNRAS, 458, 3479
McGehee P. M., 2008, Star Formation and Molecular Clouds at High Galactic Latitude. p. 813
Meng F., Wu Y., Liu T., 2013, ApJS, 209, 37
Mitchell G. F., Johnstone D., Moriarty-Schieven G., Fich M., Tothill N. F. H., 2001, ApJ, 556, 215
Molinari S., et al., 2010, A&A, 518, L100
Montillaud J., et al., 2015, A&A, 584, A92
Moore T. J. T., Urquhart J. S., Morgan L. K., Thompson M. A., 2012, MNRAS, 426, 701
Moore T. J. T., et al., 2015, MNRAS, 453, 4264
Nettke W., et al., 2017, MNRAS, 468, 250
Padoan P., Nordlund Å., Kritsuk A. G., Norman M. L., Li P. S., 2007, ApJ, 661, 972
Parikka A., Juvela M., Pelkonen V.-M., Malinen J., Harju J., 2015, A&A, 577, A69
Planck Collaboration et al., 2011a, A&A, 536, A23
Planck Collaboration et al., 2011b, A&A, 536, A24
Planck Collaboration et al., 2016, A&A, 594, A28
Putman M. E., Peek J. E. G., Joung M. R., 2012, ARA&A, 50, 491
Rigby A. J., et al., 2016, MNRAS, 456, 2885
Rivera-Ingraham A., et al., 2016, A&A, 591, A90
Röhser T., Kerp J., Ben Bekhti N., Winkel B., 2016a, A&A, 592, A142
Röhser T., Kerp J., Lenz D., Winkel B., 2016b, A&A, 596, A94
Rumble D., et al., 2015, MNRAS, 448, 1551
Sadavoy S. I., et al., 2013, ApJ, 767, 126
Schuller F., et al., 2009, A&A, 504, 415
Simpson R. J., Nutter D., Ward-Thompson D., 2008, MNRAS, 391, 205
Tang M., et al., 2018, ApJ, 856, 141
Tatematsu K., et al., 2017, ApJS, 228, 12
Tóth L. V., et al., 2014, PASJ, 66, 17
Urquhart J. S., et al., 2014, MNRAS, 443, 1555
Urquhart J. S., et al., 2018, MNRAS, 473, 1059
Veneziani M., et al., 2013, A&A, 549, A130
Wang K., et al., 2018, Research Notes of the American Astronomical Society, 2, 2
Ward-Thompson D., et al., 2007, PASP, 119, 855
Wright E. L., et al., 2010, AJ, 140, 1868
Wu Y., Liu T., Meng F., Li D., Qin S.-L., Ju B.-G., 2012, ApJ, 756, 76
Yi H.-W., et al., 2018, ApJS, 236, 51
Yuan J., et al., 2016, ApJ, 820, 37
Zhang T., Wu Y., Liu T., Meng F., 2016, ApJS, 224, 43
Zhang C.-P., et al., 2018, ApJS, 236, 49

Author affiliations:
[1]Astrophysics Research Institute, Liverpool John Moores University, IC2, Liverpool Science Park, 146 Brownlow Hill, Liverpool, L3 5RF, UK
[2]Centre for Astrophysics Research, Science & Technology Research Institute, University of Hertfordshire, College Lane, Hatfield, Herts AL10 9AB, UK
[3]Korea Astronomy and Space Science Institute, 776 Daedeokdae-ro, Yuseong-gu, Daejon 34055, Republic of Korea
[4]East Asian Observatory, 660 N. Aohoku Place, University Park, Hilo, Hawaii 96720, USA
[5]Department of Physics, P.O.Box 64, FI-00014, University of Helsinki, Finland
[6]Institute of Astronomy and Astrophysics, Academia Sinica. 11F of Astronomy-Mathematics Building, AS/NTU No.1, Sec. 4, Roosevelt Rd, Taipei 10617, Taiwan
[7]Nobeyama Radio Observatory, National Astronomical Observatory of Japan, National Institutes of Natural Sciences, Nobeyama, Minami-maki, Minamisaku, Nagano 384-1305, Japan
[8]NRC Herzberg Astronomy and Astrophysics, 5071 West Saanich Rd, Victoria, BC V9E 2E7, Canada
[9]Department of Physics and Astronomy, University of Victoria, Victoria, BC V8W 2Y2, Canada
[10]European Southern Observatory, Karl-Schwarzschild-Str.2, D-85748 Garching bei München, Germany
[11]Department of Astronomy, Peking University, 100871, Beijing China
[12]Jodrell Bank Centre for Astrophysics, School of Physics and Astronomy, The University of Manchester, Oxford Road, Manchester M13 9PL, UK
[13]National Astronomical Observatories, Chinese Academy of Sciences, Beijing, 100012, China
[14]Key Laboratory of Radio Astronomy, Chinese Academy of Science, Nanjing 210008, China
[15]IRAP, Université de Toulouse, CNRS, UPS, CNES, Toulouse, France
[16]Max-Planck-Institut für Radioastronomie, Auf dem Hügel 69, 53121, Bonn, Germany
[17]Yunnan Observatories, Chinese Academy of Sciences, 396 Yangfangwang, Guandu District, Kunming, 650216, P. R. China
[18]Chinese Academy of Sciences South America Center for Astronomy, China-Chile Joint Center for Astronomy, Camino El Observatorio #1515, Las Condes, Santiago, Chile
[19]Departamento de Astronomía, Universidad de Chile, Camino el Observatorio 1515, Las Condes, Santiago, Chile
[20]Department of Astronomy, Yunnan University, and Key Laboratory of Astroparticle Physics of Yunnan Province, Kunming, 650091, China
[21]Harvard-Smithsonian Center for Astrophysics, 60 Garden Street, Cambridge, MA 02138, USA
[22]Jet Propulsion Laboratory, California Institute of Technology, 4800 Oak Grove Drive, Pasadena, CA 91109, USA
[23]Department of Astronomy, The University of Texas at Austin, 2515 Speedway, Stop C1400, Austin, TX 78712-1205, USA
[24]Department of Physics and Astronomy, The Open University, Walton Hall, Milton Keynes, MK7 6AA, UK
[25]RAL Space, STFC Rutherford Appleton Laboratory, Chilton, Didcot, Oxfordshire, OX11 0QX, UK
[26]Korea University of Science & Technology, 176 Gajeong-dong, Yuseong-gu, Daejeon, Republic of Korea
[27]Eötvös Loránd University, Department of Astronomy, Pázmány Péter sétány 1/A, H-1117, Budapest, Hungary
[28]Konkoly Observatory of the Hungarian Academy of Sciences, H-1121 Budapest, Kinkily Thege Miklósút 15-17, Hungary
[29]School of Space Research, Kyung Hee University, Yongin-Si, Gyeonggi-Do 17104, Korea
[30]SOFIA Science Center, Universities Space Research Association, NASA Ames Research Center, Moffett Field, California 94035, USA
[31]School of Physics & Astronomy, Cardiff University, Queens Buildings, The Parade, Cardiff, CF24 3AA, UK
[32]Institute of Astronomy, National Central University, Jhongli 32001, Taiwan
[33]Physical Research Laboratory, Navrangpura, Ahmedabad, Gujarat 380009, India
[34]Department of Physics and Astronomy, University of Waterloo, Waterloo, Ontario, N2L 3G1, Canada
[35]Institute of Physics I, University of Cologne, Zülpicher Str. 77, D-50937, Cologne, Germany
[36]European Space Astronomy Centre (ESA/ESAC), Operations Department, Villanueva de la Cañada(Madrid), Spain
[37]Department of Physics, The Chinese University of Hong Kong, Shatin, NT, Hong Kong SAR
[38]Departamento de Astronomía, Universidad de Concepción, Av. Esteban Iturra s/n, Distrito Universitario, 160-C, Chile
[39]Chinese Academy of Sciences South America Center for Astronomy
[40]Astronomy Department, University of California, Berkeley, CA 94720, USA
[41]Department of Physics and Astronomy, University College London, Gower Street, London, WC1E 6BT, UK
[42]Max-Planck-Institut für Extraterrestrische Physik, Giessenbachstrasse 1, 85748, Garching, Germany
[43]Xinjiang Astronomical Observatory, Chinese Academy of Sciences; University of the Chinese Academy of Sciences
[44]ESA/STScI, 3700 San Martin Drive, Baltimore, MD 21218 USA
[45]Department of Physics, National Tsing Hua University, Guangfu Road, East District, Hsinchu City, Taiwan
[46]Institut UTINAM, UMR 6213, CNRS, Univ Bourgogne Franche Comte, France
[47]Department of Physical Science, Graduate School of Science, Osaka Prefecture University, 1-1 Gakuen-cho, Naka-ku, Sakai, Osaka 599-8531, Japan
[48]Chile Observatory, National Astronomical Observatory of Japan, National Institutes of Natural Science, 2-21-1 Osawa, Mitaka, Tokyo 181-8588, Japan
[49]Center for Computational Sciences, The University of Tsukuba, 1-1-1, Tennodai, Tsukuba, Ibaraki 305-8577, Japan
[50]School of Physics, University of New South Wales, Sydney, NSW 2052, Australia
[51]Department of Physics, School of Science and Technology, Nazarbayev University, Astana 010000, Kazakhstan
[52]University of Leicester, Physics & Astronomy, 1 University Road, Leicester LE1 7RH, UK

[53]Department of Physics and Atmospheric Science, Dalhousie University, Halifax, NS, B3H 4R2, Canada
[54]Institute of Astronomy and Department of Physics, National Tsing Hua University, Hsinchu, Taiwan
[55]Key Laboratory for Research in Galaxies, and Cosmology, Shanghai Astronomical Observatory, Chinese Academy of Sciences, 80 Nandan Road, Shanghai 200030, China
[56]Purple Mountain Observatory, Chinese Academy of Sciences, China, Nanjing 210008
[57]Square Kilometre Array Organisation, Jodrell Bank Observatory, Lower Withington, Macclesfield, Cheshire SK11 9DL, UK
[58]Department of Earth Science and Astronomy, Graduate School of Arts and Sciences, The University of Tokyo, 3-8-1 Komaba, Meguro, Tokyo 153-8902, Japan
[59]LERMA, Observatoire de Paris, PSL Research University, CNRS, Sorbonne Universités, UPMC Univ. Paris 06, Ecole normale supérieure, 75005 Paris, France
[60]Konkoly Observatory, Research Centre for Astronomy and Earth Sciences, Hungarian Academy of Sciences, H-1121 Budapest, Konkoly Thege Miklós út 15-17, Hungary
[61]Physikalisches Institut, Universität zu Köln, Zülpicher Str. 77, D-50937 Köln, Germany
[62]CSIRO Astronomy and Space Science, PO Box 76, Epping NSW, Australia
[63]Xinjiang Astronomical Observatory, Chinese Academy of Sciences; University of the Chinese Academy of Sciences
[64]Astronomy Department, Abdulaziz University, PO Box 80203, 21589, Jeddah, Saudi Arabia
[65]UK Astronomy Technology Center, Royal Observatory, Blackford Hill, Edinburgh EH9 3HJ, UK; Institute for Astronomy, University of Edinburgh, Royal Observatory, Blackford Hill, Edinburgh EH9 3HJ, UK
[66]School of Physics and Astronomy, Queen Mary University of London, Mile End Road, London E1 4NS, UK
[67]Hiroshima Astrophysical Science Center, Hiroshima University, Kagamiyama, Higashi-Hiroshima, Hiroshima 739-8526, Japan
[68]Department of Physical Science, Hiroshima University, Kagamiyama, Higashi-Hiroshima 739-8526, Japan
[69]Department of Physics and Astronomy, Seoul National University, Gwanak-gu, Seoul 08826, Korea
[70]Korea University of Science and Technology, 217 Gajeong-ro, Yuseong-gu, Daejeon 34113, Republic of Korea
[71]Department of Earth Sciences, National Taiwan Normal University, 88 Sec. 4, Ting-Chou Road, Taipei 116, Taiwan
[72]Department of Physics and Astronomy, McMaster University, Hamilton, ON L8S 4M1 Canada
[73]Department of Physics, The Chinese University of Hong Kong, Shatin, New Territory, Hong Kong, China
[74]Infrared Processing Analysis Center, California Institute of Technology, 770 South Wilson Ave., Pasadena, CA 91125, USA
[75]School of Astronomy and Space Science, Nanjing University, Nanjing 210023, China
[76]Astrophysics Group, Cavendish Laboratory, J J Thomson Avenue, Cambridge CB3 0HE, UK
[77]Graduate School of Informatics and Engineering, The University of Electro-Communications, Chofu, Tokyo 182-8585, Japan
[78]Department of Physics and Astronomy, Graduate School of Science and Engineering, Kagoshima University, 1-21-35 Korimoto, Kagoshima 890-0065, Japan
[79]Jeremiah Horrocks Institute for Mathematics, Physics & Astronomy, University of Central Lancashire, Preston PR1 2HE, UK
[80]IAPS-INAF, via Fosso del Cavaliere 100, 00133, Rome, Italy
[81]International Centre for Radio Astronomy Research, Curtin University, GPO Box U1987, Perth, WA 6845, Australia
[82]Aix Marseille Université, CNRS, LAM (Laboratoire d'Astrophysique de Marseille) UMR 7326, F-13388, Marseille, France